An innovative carrier for the formulation of amorphous solid dispersion by hot-melt extrusion with no further downstream processes: a case study with indomethacin

Suenia de Paiva Lacerda, Sylvie del Confetto, L. Haurie, M. Bernard, S. Faget, Maria-Inês Ré

An innovative carrier for the formulation of amorphous solid dispersion by hot-melt extrusion with no further downstream processes: a case study with indomethacin.

S.P Lacerda[a], S. Del Confetto[a], L. Haurie[a], M. Bernard[b], S. Faget[b] and M.I Ré[a]

[a]Centre RAPSODEE, Université de Toulouse, Albi, France; [b]Research and Development, Seppic, Paris, France

ABSTRACT

The aim of this work was to study the possibility to use Sepitrap™ as a carrier for the formulation of amorphous solid dispersions by HME (hot melt extrusion) processing aiming solubility enhancement of poorly water-soluble drugs. Sepitrap™ is a microencapsulated powder solubilizer designed to simplify the manufacture of drugs in oral solid forms, not yet tested for this purpose. The performance of Sepitrap™ was evaluated in HME processing for amorphous solid dispersions of poorly-water soluble drugs with indomethacin as a model drug. The study was conducted using a twin-screw extruder, two compositions of Sepitrap™ and different loads of indomethacin, demonstrating that Sepitrap™ could represent a new range of carriers for amorphous solid dispersions for HME processing, reducing necessary downstream steps such as grinding.

1. Introduction

Poor aqueous solubility of an API (Active Pharmaceutical Ingredient) can be addressed with various particle technologies (Zhang et al. 2018; Ambrus et al. 2022), among them supersaturated solid forms such as an amorphous solid dispersion (ASDs). ASDs are a solid dispersion in which the API is dispersed within an excipient matrix in a substantially amorphous form (Pandi et al. 2020). ASDs can also contain additional excipients, such as surfactants and/or additional polymers to further enhance drug release and stability (Vo et al. 2013; Pandi et al. 2020). The supersaturation is reached from the dissolution of these forms in the aqueous biological medium (as compared to crystalline form). To get the benefits from the supersaturated state it must be maintained for a sufficient time to favor absorption. ASDs are not new forms however the number of marketed products is still limited.

A successful development of ASDs formulation depends on three primary factors: active pharmaceutical ingredients physicochemical properties, stabilizing carrier, and processing technology. Polymers, as the most common stabilizing carriers, provide the basic and essential foundation for a stable drug amorphization, and the process supplies the energy required to transform the system to an amorphous form. The effectiveness of the process is critical to generate, capture, and preserve the amorphous form. Its success is dependent on the processing time and the supersaturation conditions that are being generated during the formation of the solid dispersion.

During ASDs downstream processing, there is often a risk of drug crystallization, especially during operations that expose the ASDs to moisture, thermal or mechanical stress (Rumondor et al. 2009; Yang et al. 2014; Luebbert and Sadowski 2017). The crystallization of a drug from ASDs during transport and storage due to the mechanical activation by grinding or crushing has also been frequently observed (Német et al. 2008). Therefore, ideal ASDs requires minimal downstream unit operations. However certain downstream processes might be inevitable. Depending on the manufacturing method, ASDs can be in the form of a fine powder, granule, extrudate or fiber. Processes like spray drying and milling usually generate fine ASDs powders that require further densification (or granulation) to enhance their density and flow properties for efficiently manufacturing their final market dosage forms (Davis et al. 2018).

Hot melt extrusion (HME) is a widely used process in different sectors of application. This technology consists in extruding two or more components at high temperatures and under mechanical mixing. In the pharmaceutical field, this technology is generally applied for the formulation of amorphous solid dispersions aiming to enhance the solubility of poorly water-soluble drugs. HME generates extrudates (usually spaghetti-shaped), which need to be milled into granules.

Considering the interest in minimizing the downstream steps after HME processing, this study was carried out to develop ASDs with a new carrier for HME process, Sepitrap™, has yet not been tested for this purpose. Sepitrap™ is a microencapsulated powdered solubilizer designed to simplify the manufacturing of drugs in oral solid forms (El-Setouhy et al. 2015; Jagtap et al. 2021). Sepitrap™ drug master file (DMF) Type IV (excipients) for pharmaceutical products is listed by Food and Drug Administration Federal Regulatory Agency. Type IV DMF concerns the development of safety profiles to support use of new excipients as components of drug or biological products. It could represent a new range of carriers for ASDs that can be easily used in HME process, reducing necessary downstream steps such as grinding. In this study the performance of Sepitrap™ was evaluated in HME processing for solubility enhancement of a poorly-water soluble model BCS (Biopharmaceutical Classification System) Class II drug

Indomethacin (IND) by forming amorphous solid dispersions. The effects of formulation variables (compositions of Sepitrap™80 and load of indomethacin) on the different physicochemical characteristics of ASDs were investigated.

This study was performed in three different stages:

- Characterization of the innovative excipients (Sepitrap™-F20 and Sepitrap™-F50) on its physical characteristics (particle morphology and size, specific surface area and volume of pores, crystallinity) and extrudability.
- Investigation of the impact of different drug loads on the Sepitrap™/IND extrudate manufacturability with one of the compositions studied here (Sepitrap™-F50).
- Production and characterization of Sepitrap™/IND extrudates with two different grades of Sepitrap™ (Sepitrap™-F20 and Sepitrap™-F50) at a quite high drug load (around 42-44%wt).

2. Materials and Methods

2.1. Materials

Indomethacin (MW 357.79 g/mol; 98% of purity) (IND) was purchased from Alfa-Aesar (Thermofisher, Massachusetts, USA). Sepitrap™ and polysorbate 80 were kindly provided by Seppic (France). For high-performance liquid chromatography (HPLC), Acetonitrile (ACN) and Acetic acid HPLC grade were bought from Avantor, Radnor, USA and Merck, Darmstadt, Germany respectively. Distilled and purified water were obtained by the purification system Milli-Q (Classic Purelab DI, MK2) (Elga, HighWycombe, UK).

2.2. Methods

2.2.1. HME processing of binary mixtures IND and Sepitrap™

Two formulations of Sepitrap™ were tested, a first (Sepitrap™-F50) comprising 50 wt% and a second (Sepitrap™-F20) containing 20 wt% of liquid polysorbate 80 adsorbed onto a porous magnesium aluminosilicate support during manufacturing process. Different extrudate granules (EG) with both Sepitrap™ grades and different IND loads were produced. EG samples were produced by HME process performed using a Thermo-Fisher Pharma 16 Extruder (Thermo scientific™, Karlsruhe, Germany). The equipment is composed of a co-rotating twin-screw with 16 mm and L (barrel length)/D ratio equal to 40. The screw speed was fixed at 100 rpm. The process temperature was set up at 180 °C and at 50 °C in the terminal zone. The extruder barrel was divided into eight heating zones (Z) and two mixing zones. The heating and mixing zones of the extrusion were adjusted to ensure desirable melting and optimal mixing during extrusion.

Physical mixtures (PM) of the same mass compositions as EG were also produced for comparison purposes. Sepitrap™-F20/IND and Sepitrap™-F50/IND at 40% wt IND were mixed in a Turbula™ mixer (T2F mixer, WAB Group, Switzerland) for 3 min at 96 rpm.

2.2.2. Characterization of Sepitrap™ and Sepitrap™/IND extrudate granules

2.2.2.1. Particle size. Particle size measurements were performed with a Mastersizer 3000 granulometer (Malvern Instruments, Malvern, UK), using a dry dispersion unit. Average particle size was expressed as the volume mean diameter D [4;3]. Polydispersity was given by Span index calculated by $(Dv_{90} - Dv_{10})/Dv_{50}$, where Dv_{90}, Dv_{50} and Dv_{10} are the particle diameters determined respectively at the 90th, 50th and 10th percentiles of undersized particles. Measurements were carried out in triplicate.

2.2.2.2. Scanning electronic microscopy (SEM). SEM images were obtained using a scanning electron microscope HITACHI TM3030 Plus (Hitachi, Tokyo, Japan) equipped with an X-ray microanalysis probe. Samples were fixed on a support using a double-sided adhesive tape. Each sample was observed in two modes, with an acceleration voltage of 15 kV: the "low vacuum" mode which allows to obtain information of chemical composition and the "standard" mode which allows to obtain information of topography.

2.2.2.3. Brunauer emmett and teller (BET) analysis. BET analysis was performed on a 3Flex equipment from Micromeritics (USA). Prior to the measurement, the samples were submitted to a degassing step at 90 °C for 1h, then the temperature was increased at a rate of 5 °C/min to 150 °C for 10h. Nitrogen adsorption isotherm was performed at nitrogen temperature of 77 K up to a relative pressure of 1. The specific surface area was calculated by applying the BET model in the appropriate pressure range. The size pores distribution is given by Barrett-Joyner_Halenda (BJH) method.

2.2.2.4. X-ray powder diffraction (XRPD) analysis. Powder diffractograms were obtained using a Philips X'Pert Panalytical X-ray diffractometer (Malvern Panalytical, Malvern, UK) with Cu$K\alpha$ radiation, 40 mA of current, and 45 kV of voltage. The recording spectral range was set at 6–45° with a measuring step (angular deviation between 2 consecutive points) of 0.033° and an acquisition time of 22.23s per point. Each sample to be analyzed was introduced in a sample holder and rotated (1 revolution/s) during the results acquisition.

2.2.2.5. Differential Scanning calorimetry (DSC). The thermal analyses were performed using a DSC Q200 (TA instruments, New Castle, DE, USA). For raw materials, the analysis was carried out in a temperature range from 10 up to 170 °C (heating rate 10 °C.min^{-1}) under nitrogen flow rate of 50 ml.min^{-1}. An RCS90 cooling system was used to precisely control the cooling rate. Samples were placed in non-hermetic aluminum pans and an empty aluminum pan was used as reference. The EG with IND were analyzed using the Modulated DSC (MDSC) mode, which is able to detect more complex thermal events such as API glass temperatures (Tg). For modulated mode the analysis was performed in a temperature range from 10 up to 200 °C (heating rate 2 °C.min^{-1}), the modulation period was of 60 s and the modulation amplitude was 1.2 °C.

2.2.2.6. Determination of drug loading. IND quantification was carried out in duplicate dissolving 15 mg of IND in mobile phase 50:50 w/w (ACN:Water) to obtain a final concentration of 0.15 mg/g. Each sample of solution was then filtered through a 0.22 μm polypropylene (PP) filter (VWR, Fontenay- sous-Bois, France). API assay was performed by high-performance liquid chromatography (HPLC). The HPLC system (Agilent 1100 Series, France) was composed of a reversed phase column ProntoSIL Eurobond C18 (100 mm × 4.6 mm, 10 μm) and an UV detector set at 318 nm. The column was stored in an oven at room temperature (25 °C). Isocratic mobile phase was ACN and acetic acid (50:50 v/v), the injection volume was 20 μL, the flow rate of 1.0 ml/min and the retention time was 5.3 min.

2.2.2.7. Solubility measurement. Solubility was determined by equilibrating an excess of IND in 30 g of phosphate buffer pH 7.2. Each experiment was carried out in duplicate. Sealed flasks were

maintained under stirring at 37 ± 0.5 °C in a temperature-controlled bath up to 48h. Solution aliquots were withdrawn at different time points filtered through 0.22 µm cellulose acetate syringe filters (VWR, Fontenay- sous-Bois, France) and then the concentration of dissolved IND was determined by HPLC method as described before.

2.2.2.8. In vitro drug release studies. Drug release profiles of physical mixture and EG samples were performed using a USP-II paddle apparatus (DT 60) (ERWEKA, Heusenstamm, Germany). Paddle speed of 100 rpm and temperature of 37 ± 0.5 °C were set for each test. To ensure SINK conditions ($C_{saturation} \gg C_{solution}$, See European Pharmacopeia- 5.17.1), based on measured equilibrium concentration of 1.5 mg/g, the samples (50 mg) were dispersed into the dissolution vessel with 1000 ml of phosphate buffer pH7.2 media. During the dissolution test, aliquots of 3 ml were sampled at 5, 10, 20, 30, 60, 120 and 180 min, filtered through 0.22 µm cellulose acetate syringe filters. IND release was measured by HPLC as described before. The dissolution tests were performed in duplicate.

2.2.2.9. Monitoring Sepitrap™/IND EG stability upon storage. Sepitrap™/IND_EG samples were stored in a Memmert HPP110 climatic chamber (Memmert, Schwabach, Germany) at 40 °C and 75% relative humidity (RH). The samples were packaged in open glass vials. Physical and chemical evolution of the samples was followed at different time points (T_0Week, T_4Weeks, T_{12}Weeks) by physicochemical characterizations and solubility determination.

3. Results and discussion

3.1. Characterization of SepitrapTM-F20 and SepitrapTM-F50

3.1.1. Morphology and particle size

According to SEM images of Sepitrap™-F20 and Sepitrap™-F50 (See Figure 1) the particles possess a very similar shape, mostly spherical. At a microscopic scale, there is a slight difference between both excipients on particle surface morphology that can be related to the amount of Polysorbate 80 on the particle surface.

Table 1 shows the characteristic diameters for Sepitrap™ grades obtained from laser diffraction granulometry. Both samples are characterized by close particle size distribution with a fine fraction of particles, which corresponds to the D_{v10} values, of 3.7–3.9 µm, while the largest fraction D_{v90} gives 140-155.5 µm, revealing a broad particle size distribution (span > 2).

3.1.2. Specific surface area and pore size from nitrogen sorption isotherms

A reduction of the specific surface area and of the volume of mesopores is observed with the increase of the concentration of polysorbate 80 in Sepitrap™ (Table 2), as illustrated in Figure 2 for pore volume comparison. According to IUPAC classification, the nitrogen adsorption isotherms shows that Sepitrap™-F20 is a mesoporous solid (type IV isotherm), whereas this mesoporosity is no longer present in Sepitrap™-F50 (type II isotherm) (data not shown). The impact of the surfactant content in Sepitrap™ samples is clearly visible by this analysis, and this may influence the stabilization of the active ingredient after hot melt extrusion.

3.1.3. Solid state characterization

3.1.3.1. DSC and XRPD analysis. Sepitrap™-F20 and Sepitrap™-F50 show similar thermal behavior between 0 °C and 200 °C without thermal events associated with solid state transformations, as shown in Figure 3. The large endotherm peak observed between 20 °C and 110 °C, more visible for Sepitrap™-F50, was associated with water evaporation. Figure 4 shows the X-ray diffractograms of Sepitrap™-F20 in comparison to that of Sepitrap™-F50. They show a broad and diffuse halo characteristic of amorphous materials. The main substance of Sepitrap™ is composed of amorphous silicate phase. The slight Bragg angle around 2θ at 22°, is consistent with previous studies that amorphous silicate phase has a hump between 15 to 35°of 2θ (Morsi and Mohamed 2018; Prasetyo et al. 2022).

3.1.3.2. Extrudability of Sepitrap™ grades. To evaluate the extrudability of Sepitrap™-F50 and Sepitrap™-F20, preliminary series of experiments were performed in search of extrusion conditions that do not modify the physical characteristics (particle size distribution) of the Sepitrap™ samples (no grinding).

Process feasibility results (data not shown) were able to confirm that the extrusion of Sepitrap™ alone, regardless of the

Table 1. Characteristic diameters of Sepitrap™ samples determined by laser granulometry ($n = 3$).

Sample	D_{v10} (µm)	D_{v50} (µm)	D_{v90} (µm)	D[4;3] (µm)	Span
Sepitrap™ -F20	3.9 ± 0.1	60.0 ± 0.4	155.5 ± 2.1	70.7 ± 0.6	2.5
Sepitrap™ -F50	3.7 ± 0.1	60.3 ± 0.2	140.0 ± 1.4	66.4 ± 0.2	2.3

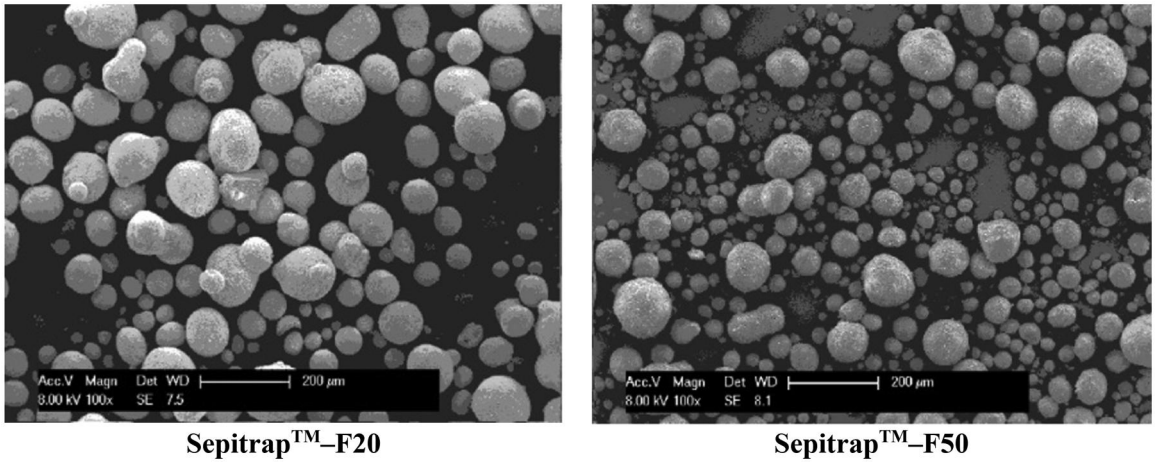

Sepitrap™–F20 Sepitrap™–F50

Figure 1. SEM images of Sepitrap™-F20 and Sepitrap™-F50.

Table 2. BET results obtained by nitrogen sorption at 77K (raw materials and Sepitrap^{TM}/IND_EG samples).

Samples		BET	BJH	
Code	IND content (%wt)[a]	surface area (m^2/g)	Vmeso(cm^3/g)[b]	PD[c](nm)
Sepitrap^{TM}-F20	–	244.3	0.87	12.4
Sepitrap^{TM}-F50	–	36.2	0.24	17.8
Commercial γ-IND	98.0	2.2	–	–
Sepitrap^{TM}-F50/IND_EG_1	14.9	8.3	0.20	36.5
Sepitrap^{TM}-F50/IND_EG_2	31.2	2.9	0.05	37.5
Sepitrap^{TM}-F50/IND_EG_3	43.8	4.9	0.03	43.2
Sepitrap^{TM}-F20/IND_EG_4	42.8	101.5	0.39	13.2

[a]*HPLC Assay.*
[b]*Vmeso : Volume mesopores.*
[c] *PD;: Pores Diameter Mean.*

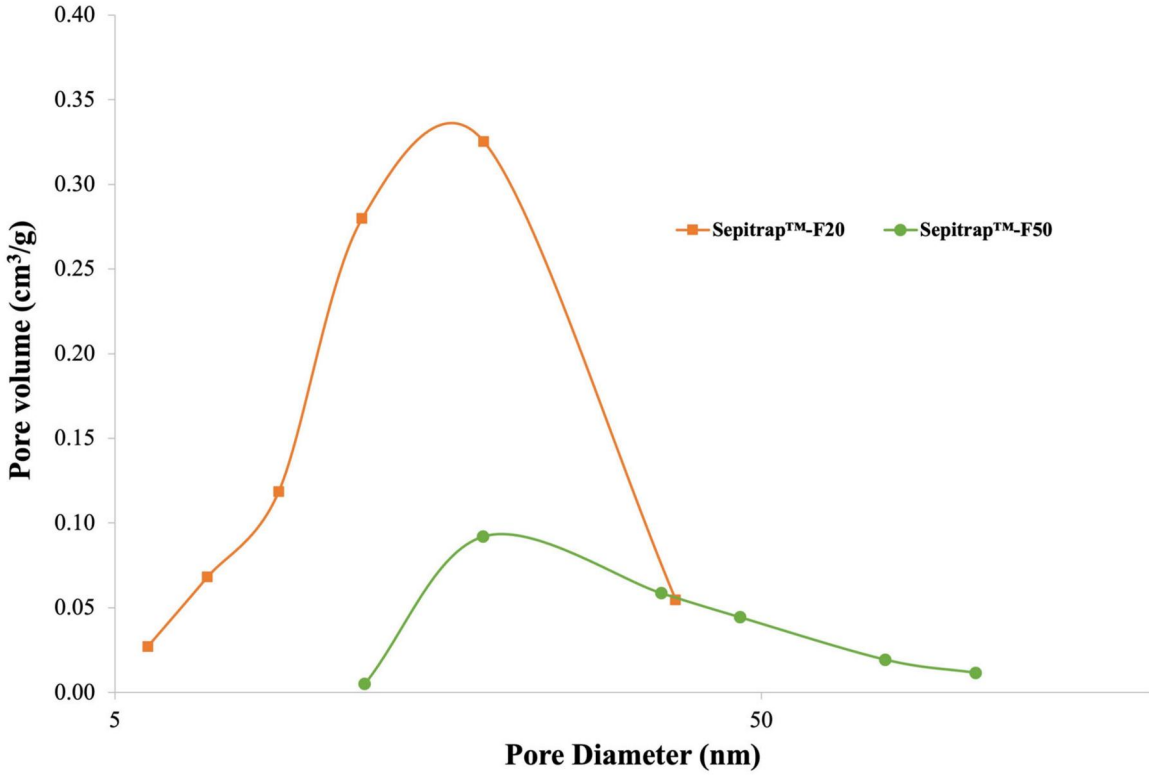

Figure 2. BJH pore size distribution for Sepitrap^{TM}-F20 and Sepitrap^{TM}-F50.

chosen screw profile, did not modify their physical characteristics (shape and size, confirmed by particle size and SEM analyses). The presence of surfactant in the pore and at the surface of the particles probably acts as a lubricant against mechanical friction, confirming the great adaptability of this raw material for HME processing.

4.2. HME processing of SepitrapTM-F50 with different drug (IND) loads

Sepitrap^{TM}-F50/IND_EG with three different drug loads were produced: 14.9%wt (Sepitrap^{TM}-F50/IND_EG_1), 31.2%wt (Sepitrap^{TM}-F50/IND_EG_2), and 43.8%wt (Sepitrap^{TM}-F50/IND_EG_3).

4.2.1. Gas adsorption for surface area and pore size analysis

Nitrogen sorption isotherms were performed on the EG after HME processing to provide information about the impact of drug load on the surface area of the extrudate granules. The data in Table 2 shows a decrease in specific surface area and pore volumes with increasing IND content. For the extrudates of Sepitrap^{TM}-F50 with IND $\geq$ 31.2%wt (Sepitrap^{TM}-F50/IND_EG_2 and Sepitrap^{TM}-F50/IND_EG_3), the pore volume almost completely disappeared.

4.2.2. Solid state characterization

Figure 5 shows the MDSC thermograms of Sepitrap^{TM}-F50 IND_EG samples. The MDSC thermograms obtained for unprocessed IND and for the surfactant present in Sepitrap^{TM} were also displayed in Figure 5B. The thermal profile of unprocessed IND crystals shows a distinct onset melting endotherm (Tm_{onset}) at 159.7 °C with a ΔHm of 125.2 J/g. This value of Tm_{onset} is close to that reported in the literature for the crystalline form of γ-IND (Xu et al. 2018). The second cycle of heating (DSC curve not shown) revealed a glass transition (Tg) of 46.0 °C and a corresponding heat capacity (Cp) of 0.5 J/g °C for the amorphous form of IND.

On all Sepitrap^{TM}-F50/IND_EG samples, there is no visible Tg over the temperature range studied (even on revHF shown in Figure 5C for Sepitrap^{TM}-F50/IND_EG_3). An endotherm found around 100–104 °C (Figures 5(B and C) is probably an event coming from the presence of the surfactant in Sepitrap^{TM}-F50 (red dotted curve in Figure 5B), followed by an endotherm-exotherm-endotherm that may correspond to changes in the polymorph of

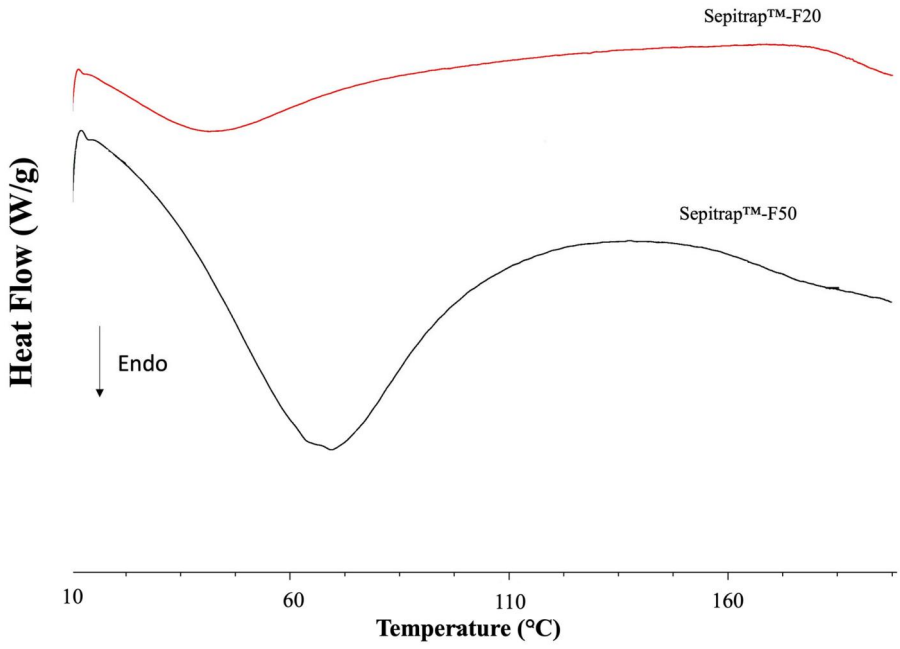

Figure 3. DSC thermograms of Sepitrap™-F20 and Sepitrap™-F50.

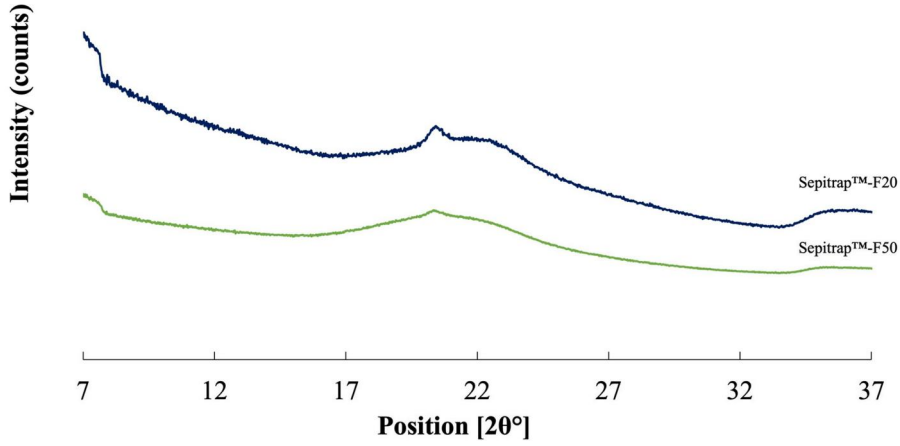

Figure 4. X-ray diffractograms of Sepitrap™-F20 and Sepitrap™-F50.

IND around 132 °C (fusion of δ – IND) and around 149 °C (crystallization of the δ form into γ or α form then fusion of the form obtained). Table 3 regroups the Tm and Tg data from all DSC thermograms. For comparison, the physical mixture for Sepitrap™-F50/IND_EG$_2$ (before HME processing) was also analyzed and exhibited an endotherm at 157.6 °C corresponding to the γ-IND crystalline form.

XRPD analysis has provided more information related to crystalline traces. XRPD analyses were performed on the three Sepitrap™-F50/IND_EG, immediately after HME processing (T0). The x-ray diffractograms are presented in Figure 6. The XRPD analysis performed on Sepitrap™-F50/IND_EG$_1$ shows some very weakly crystallized compound at T0, which could not be identified due to very weak signals. The peaks which appear in the DRX diffractogram of Sepitrap™-F50/IND _EG$_2$ and Sepitrap™-F50/IND _EG$_3$ are: 16.0 (more intense), 10.5, 12.1, 17.4, 18.4, 20.1 and 21.2 degrees.

It has been reported that IND exists in 8 polymorphic forms α, β, γ, δ, ε, ξ, η and τ (Okumura et al. 2006; Surwase et al. 2013; Van Duong et al. 2018). The peak positions for the different polymorphs identified in the literature are regrouped in Table 4. The form ε is not stable enough to obtain a diffractogram. The form γ is the thermodynamically stable polymorph while the form α is the most observed metastable form. The commercial indomethacin (IND) used (see Figure 6) is the γ form.

According to the peak positions for the different IND polymorphs identified in the literature (Table 4), the polymorph in Sepitrap™-F50/IND _EG$_2$ is IND τ or a mixture of the 2 polymorphs α and τ. Four polymorphic forms were identified in the weakly crystallized Sepitrap™-F50/IND _EG$_3$: α (8.5; 11.9; 14.4; 18.5 and 22.0 degrees), γ (10.2 degrees), δ (10.5 degrees) and τ (16.2 degrees).

4.2.3. Solubility measurements

The IND equilibrium concentration in phosphate buffer pH 7.2. at 37 °C was achieved at 24 h (Figure 7). With 14.9%, 31.2% and 43.8% wt of IND the behavior was similar: a gain in apparent solubility with values 1.5 times greater than the equilibrium

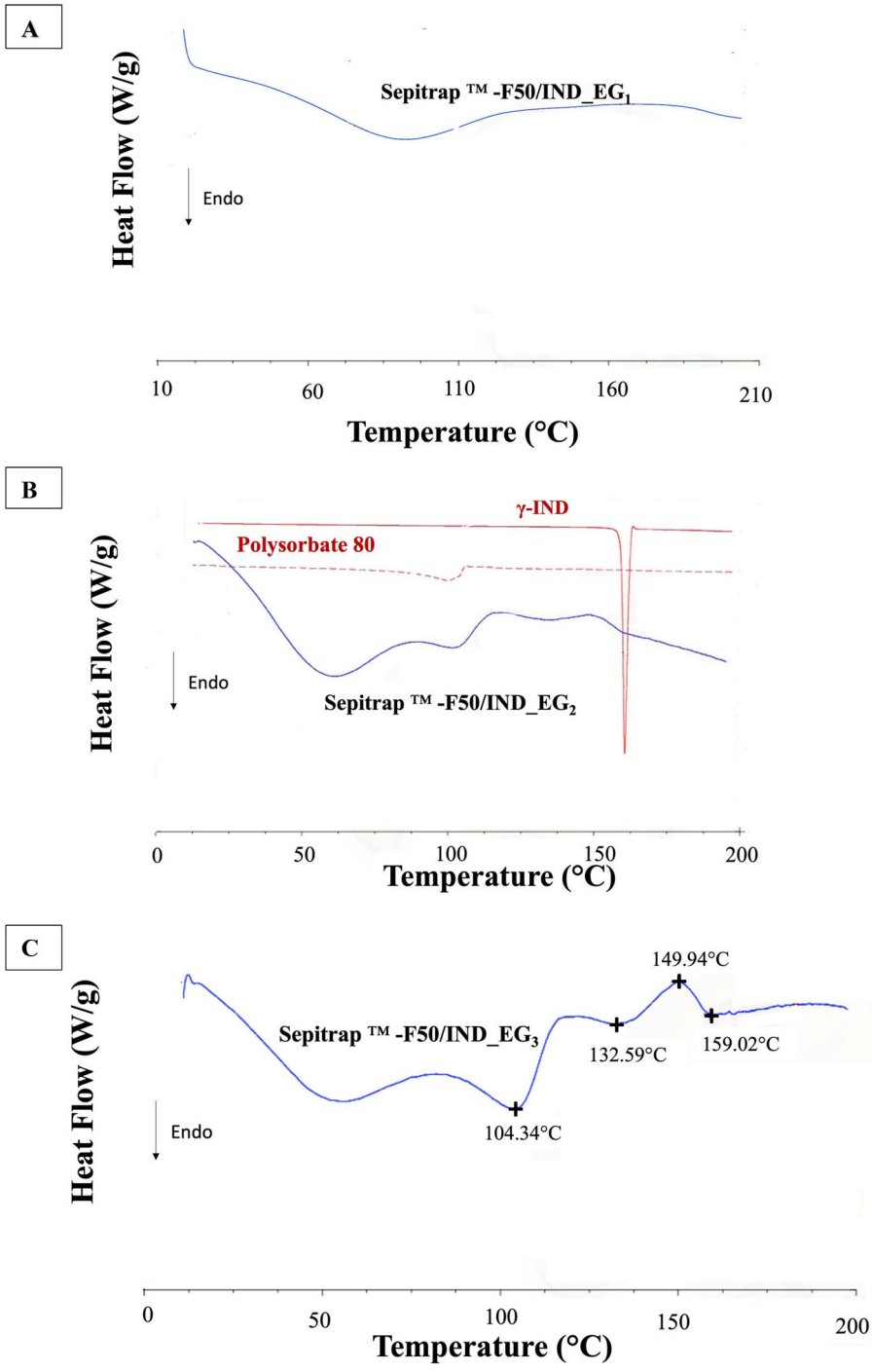

Figure 5. DSC thermograms for Sepitrap™-F50/IND_EG samples freshly produced: A) Sepitrap™-F50/IND_EG$_1$ (1st heating cycle); B) SepitrapT^M-F50/IND_EG$_2$ (1st heating cycle); C) Sepitrap™-F50/IND_EG$_3$ (MDSC).

concentration with the raw IND, which remained stable until the end of the experiment. The effect in the first hour observed in Figure 7 in comparison to the raw IND can be partly attributed to the effect of the surfactant present in the formulation in accelerating IND dissolution rate, however it did not alter the solubility of γ-IND in the buffer phosphate medium pH 7.2 at 37 °C, as checked experimentally (data not shown). The main effect on the IND concentration in the medium can be due to the transformation of its solid state (crystallinity decrease, IND polymorphs mixture) during HME processing.

4.2.4. Dissolution kinetics

Figure 8 presents the dissolution kinetics profiles of commercial and extrudate samples. Dissolution rate improvement was noticed on solid dispersions generated with Sepitrap™-F50. This improvement is more evident in the first 60 min, and it is directly proportional to the amount of Sepitrap™-F50 in the extrudates, which accelerates IND dissolution rate, as discussed previously. In addition, the curves revealed an IND immediate release profile in the dissolution medium for extrudates containing 14.9%, 31.2% and 43.8% wt of IND respectively. For immediate release (IR) solid oral

Table 3. Experimental Tm_{onset} and Tg temperatures obtained from DSC curves.

		Heating Cycle 1		Heating Cycle 2	
Sample	Thermal event	Tm_{onset} (°C)	ΔH fusion (J/g)	Tg (°C)	ΔCP (J/g.°C)
Commercial γ-IND	Fusion γ	159.6	125.2	45.2	0.56
Sepitrap™-F50	–	–	–	–	–
Sepitrap™-F50/IND_EG$_1$	Difficult to integrate				
Sepitrap™-F50/IND_EG$_2$		155.7	0.52	–	–
Sepitrap™-F50/IND 40% wt – PM[a]	Fusion γ	157.6	28.30	–	–
	Fusion α	–	–	–	–
	Tg	–	–	–	–
	Recryst.[a]	–	–	–	–
Sepitrap™-F50/IND_EG$_3$	Fusion γ	159.1	0.56	–	–
	Fusion δ	131.5	1.91	–	–
	Fusion α	143.0	0.19	–	–
	Tg	–	–	–	–
	Recryst.[a]	-/149	-/0.13	–	–

[a]*PM: Physical Mixture; Recryst.: recrystallization.*

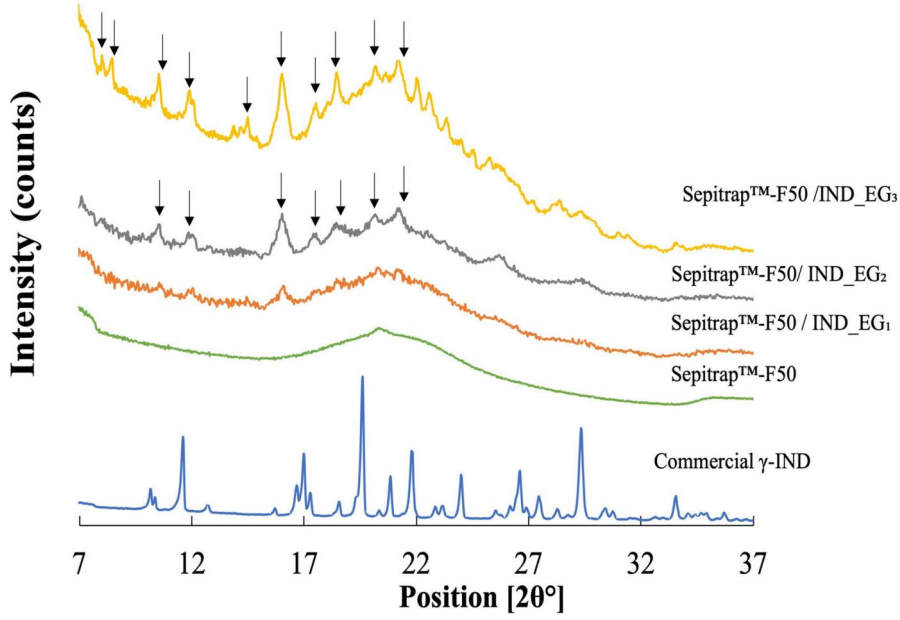

Figure 6. X-ray diffractograms of Sepitrap™-F50/IND_EG immediately after HME processing.

Table 4. Peak positions (2) for the different IND polymorphs identified in the literature (adapted from Van Duong et al. 2018).

IND Polymorphic form	Position of the diffraction peaks in 2θ (deg)
γ	10.2, 11.7, 16.7, 19.6, 20.5, 21.9 (Van Duong et al. 2018) 11.6, 16.7, 19.6, 21.9 et 26.7 (Okumura et al. 2006)
α	6.9, 8.5, 11.5, 11.9, 13.9, 14.2 17.6, 18.0 (Van Duong et al. 2018) 8.4, 14.4, 18.5, 22.1 (Okumura et al. 2006)
τ	4.1, 5.4, 6.0, 7.4, 8.2, 10.6, 12.3, 16.5, 17.7, 18.2 (Van Duong et al. 2018)
δ	9.6, 10.5, 11.3, 13.0, 14.9 (Surwase et al. 2013)
ξ	6.5, 11.0, 11.8, 12.8, 14.4, 16.4 (Surwase et al. 2013)
η	9.1, 9.3, 12.2, 18.2, 20.5 (Surwase et al. 2013)

drug products, one dissolution criterion is at least 80% of dissolved drug in 30 min (FDA, 2018).

5.3. Production and characterization of Sepitrap™/IND extrudates with two different grades of Sepitrap™ (Sepitrap™-F20 and Sepitrap™-F50) at a close drug load (around 42-44%wt)

Aiming to compare Sepitrap™/IND extrudates prepared with Sepitrap™ with different compositions (load of Polysorbate 80), a new sample was produced: Sepitrap™-F20/IND_EG$_4$ with IND load of 42.8%wt, determined by HPLC. It was compared to Sepitrap™-F50/IND_EG$_3$, the Sepitrap™-F50/IND with 43.8% wt of drug load as real value.

5.3.1. Powder Morphology and size: macroscopic and microscopic aspects

The HME processing generated a slightly yellowish powder and did not result in the formation of aggregates as shown by the pictures in Figure 9 and thus no further micronization was required. The particles of the extruded products are in the same size range of the particles of Sepitrap™ before HME processing, *i.e.* in the range 3.9 to 155 µm.

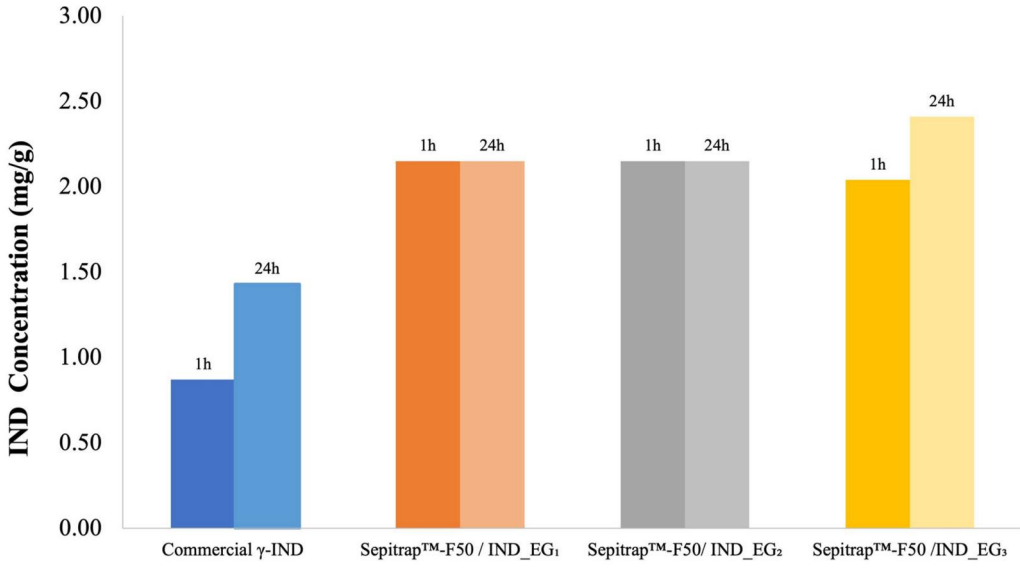

Figure 7. IND solubilization kinetics profiles over 24h. Values are presented as mean ($n = 2$).

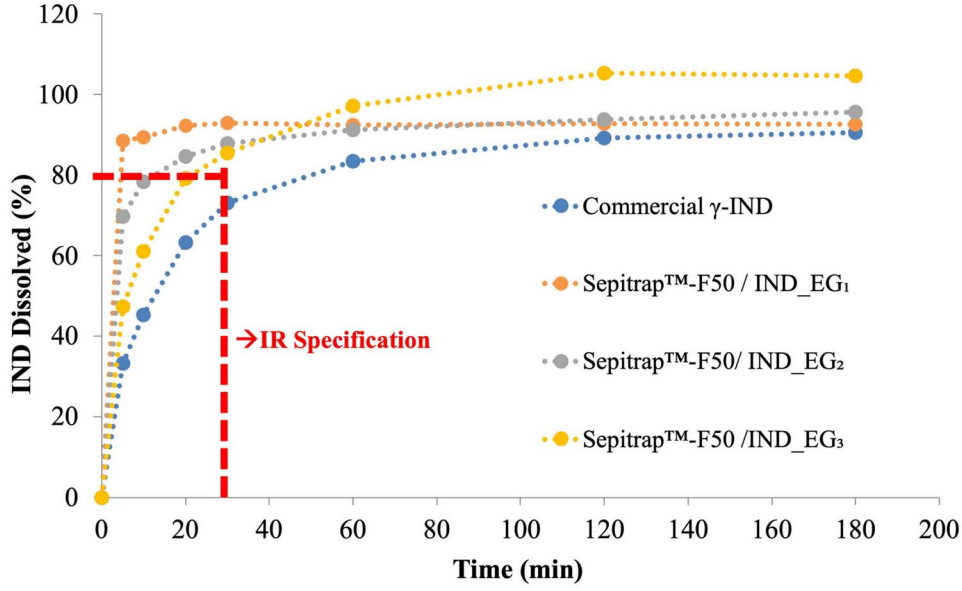

Figure 8. IND dissolution kinetics profiles in phosphate buffer pH 7.2 at 37 °C. Values are presented as mean ($n = 2$).

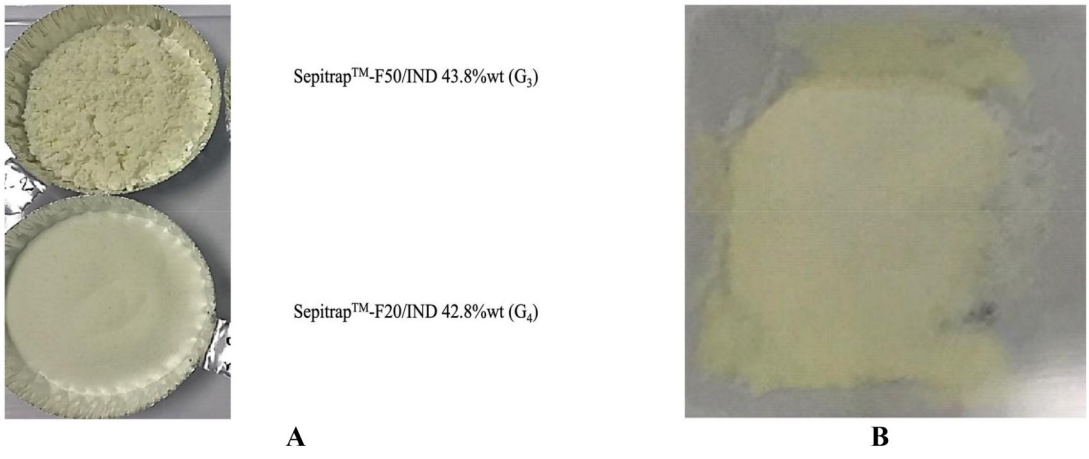

Figure 9. Extrudate powders visual aspect: A) Sepitrap™-F50/IND 43.8%wt (G_3); B) Sepitrap™-F20/IND 42.8%wt (G_4).

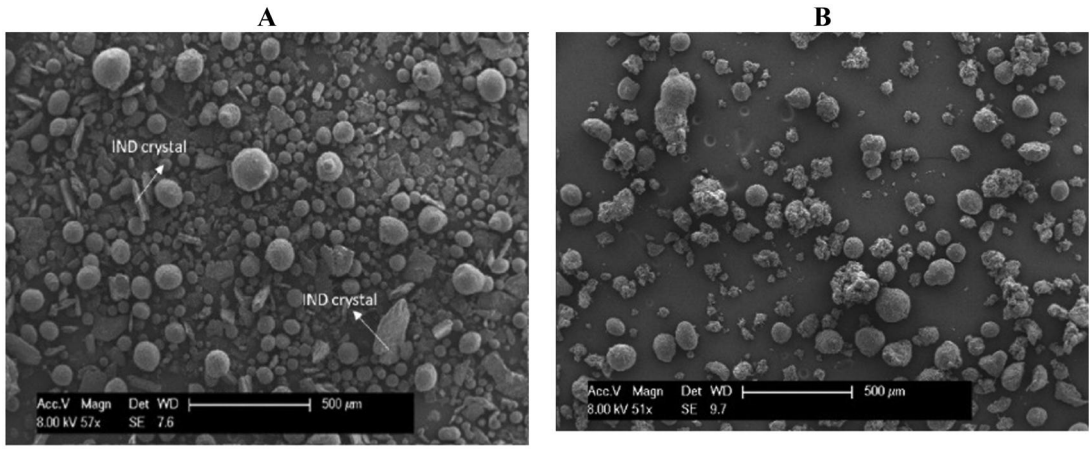

Figure 10. SEM images of Sepitrap^{TM}-F50/IND_G_3 samples: A- physical mixture; B- EG sample.

SEM images were used to examine both extruded formulations of Sepitrap^{TM}/IND. As the images are very similar, only the images of Sepitrap^{TM}-F50/IND_G_3 are shown (Figure 10) in comparison to a corresponding physical mixture. First, in a corresponding physical mixture, non-spherical raw IND particles (see Figure 10 A) were visible side by side with the Sepitrap^{TM} particles, more spherical in shape. The effect of the HME processing can be seen on the extrudates (Figure 10 B) with the disappearance of the Commercial γ-IND crystals, suggesting solid state transformation of IND during HME processing.

5.3.2. Solid state characterization

5.3.2.1. Specific surface area and pore size from nitrogen sorption isotherms. As already mentioned, a reduction of the specific surface area was observed for Sepitrap^{TM}-F50 (36.2 m^2/g) compared to Sepitrap^{TM}-F20 (244.3 m^2/g) (Table 2). The physical mixtures used to extrude Sepitrap^{TM}-F50_G_3 and Sepitrap^{TM}-F20_G_4 were also analyzed, and the corresponding surface areas were 10.5 m^2/g and 148.3 m^2/g, respectively. The theoretical specific surface areas calculation by considering the experimental specific surfaces and the contents of each compound gives respectively the values of 21 m^2/g and 140 m^2/g, which are of the same magnitude of the experimental values measured for the physical mixtures. In these cases, it cannot be concluded that the pores are filled.

On the other hand, for the extruded samples: Sepitrap^{TM}-F50_EG_3 and Sepitrap^{TM}-F20_EG_4, a decrease of the experimental specific surface is observed (4.9 m^2/g and 101.5 m^2/g, respectively), compared to the theoretical specific surface, as well as a decrease of the pore volume (see Table 2), which suggests that IND fills the pores.

5.3.2.2. XRPD analysis. XRPD analyses were performed on the new Sepitrap^{TM}-F20/IND_EG_4 immediately after HME processing (T0), and both samples (Sepitrap^{TM}-F50/IND_EG_3 and Sepitrap^{TM}-F20/IND_EG_4) were monitored by XRPD during their storage period under controlled environment conditions (40 °C, 75%RH, open vials). The XRPD diffractograms are presented in Figure 11.

As already discussed, four polymorphic forms were identified in the weakly crystallized Sepitrap^{TM}-F50/IND _EG_3: α (8.5; 11.9; 14.4; 18.5 and 22.0 degrees), γ (10.2 degrees), δ (10.5 degrees) and τ (16.2 degrees) in the diffractograms of Figure 11A.

According to the diffractograms shown in Figure 11B, Sepitrap^{TM}-F20/IND_EG_4 shows the presence of small peaks (presence of slightly crystalline IND in the α form - peaks at 8.5; 12.0; 14.4; 18.5 and 22.0 degrees - and δ to a lesser extent - peak at 9.6 degrees), similarly to Sepitrap^{TM}-F20.

In summary, the crystalline parts in the EG diffractograms shown in Figure 11 correspond to metastable forms for the most part (γ, α, δ and τ in the formulations with Sepitrap^{TM}-F50/IND_EG_3, and α and δ for those with Sepitrap^{TM}-F20/IND_EG_4). Moreover, these forms did not evolve to the γ form during accelerated storage test in contact with high relative humidity and temperature of 40 °C. It is a matter of transformation from a stable crystalline form into a probably amorphous and a metastable crystalline fraction, which are stabilized by the solid dispersion formulation with Sepitrap^{TM} products. DSC thermograms (data not shown) corroborate with these results.

5.3.3. Solubility measurements

Figure 12 shows the IND equilibrium concentration in phosphate buffer pH 7.2. at 37 °C achieved at 24 h from Sepitrap^{TM}-F20/IND_EG_4 freshly prepared (T0) in comparison to Sepitrap^{TM}-F50/IND_EG_3. These values are higher than those achieved with the commercial γ -IND and the corresponding physical mixture between γ-IND and Sepitrap^{TM} (data no shown), which can be attributed to the amorphization and/or polymorphic change of the crystalline IND form. However, it is difficult to associate a trend of solubility improvement linked to formulation composition, which can be related to different polymorphic forms present in different samples.

Figure 12 also illustrates the effect of aging on the IND equilibrium concentration from the EG stored in open vials exposed to 40 °C at 75%RH at 4 and 12 weeks. A trend toward a reduction in apparent solubility gain with exposure to aging conditions can be observed, however this effect is less for Sepitrap^{TM}-F20/IND_EG_4.

It is important to note that the samples were exposed directly to conditions of 40 °C and 75%RH and that the effect on apparent solubility will depend on these conditions. Samples of Sepitrap^{TM}-F50/IND_EG_3 and Sepitrap^{TM}-F20/IND_EG_4 were stored in parallel in closed vials at room temperature for 24 weeks. Under these conditions the reduction in the apparent solubility values measured at T0 were reduced by less than 5% for both samples (data not shown).

5.3.4. Dissolution behavior

Figure 13 compares the dissolution kinetic profiles from the samples Sepitrap^{TM}-F50/IND_EG_3 and Sepitrap^{TM}-F20/IND_EG_4 freshly produced (T0). As previously discussed, dissolution kinetics of EG

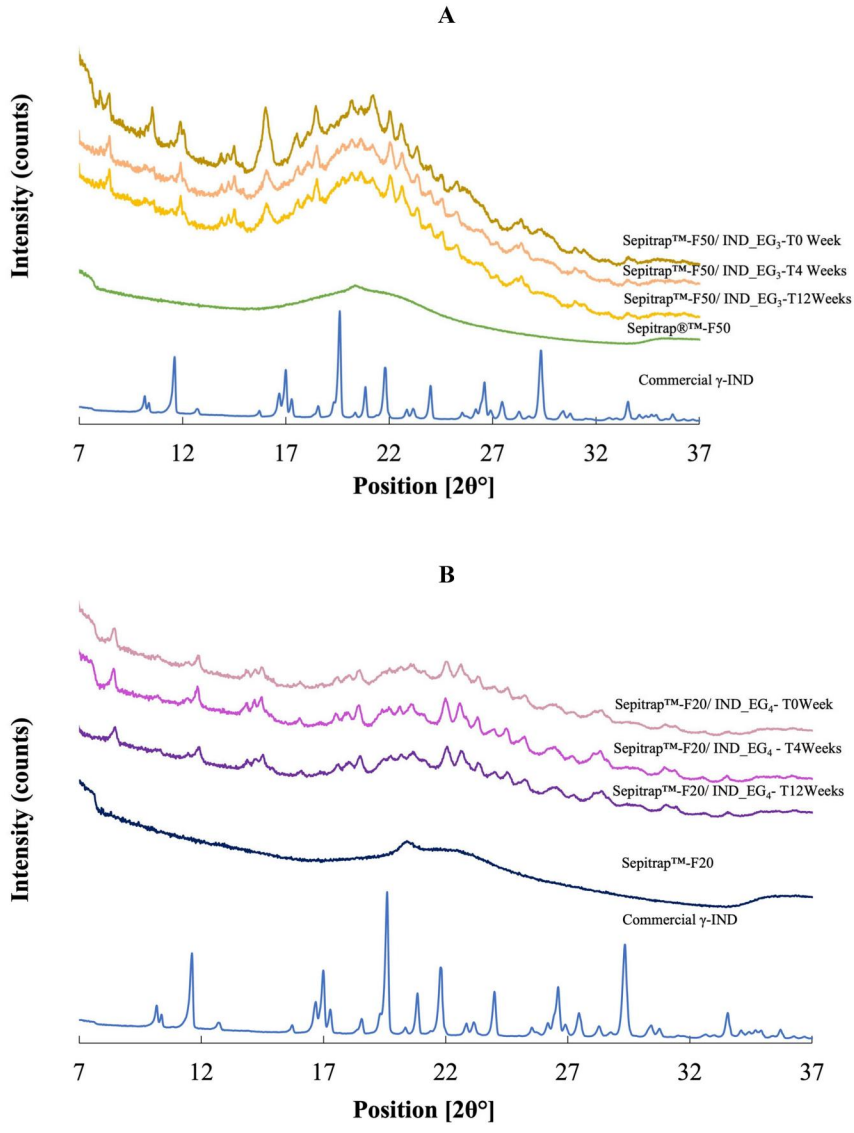

Figure 11. X-ray diffractograms at T0, T4and T12 weeks of EG samples with close loads of IND: A)Sepitrap™-F50/IND_G_3; B) Sepitrap™-F20/IND_EG_4.

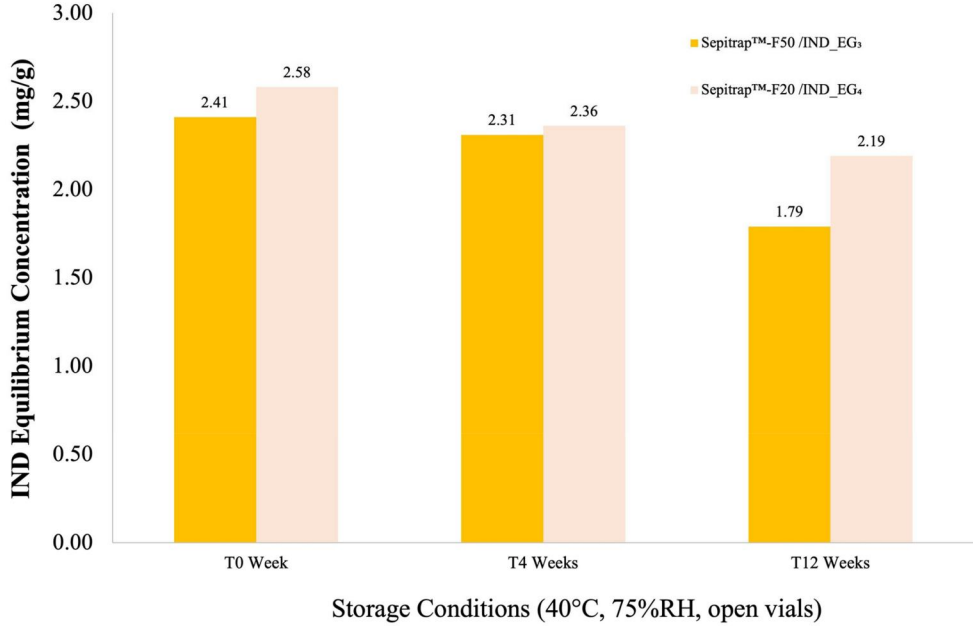

Figure 12. IND equilibrium concentration in phosphate buffer pH 7.2. at 37 °C achieved at 24 h.

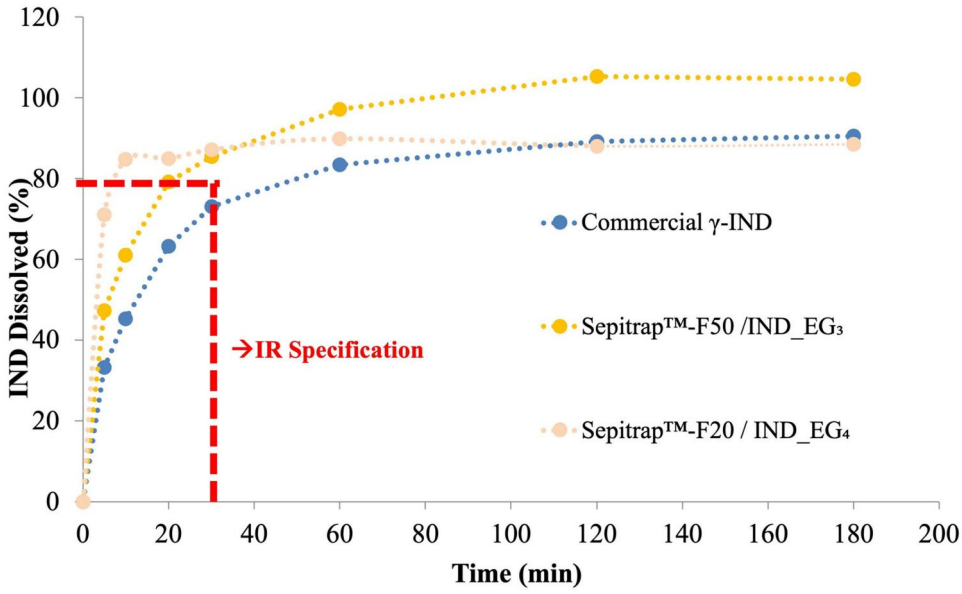

Figure 13. IND dissolution kinetics profiles in phosphate buffer pH 7.2 at 37 °C. Values are presented as mean ($n = 2$).

shows a profile of immediate release dosage form for both excipient grades (FDA 2018).

6. Conclusion

This work has demonstrated for the first time that Sepitrap™ has the physical characteristics suitable for extrusion process, where no powder physical change was observed after extrusion and the presence of surfactant in the pore and at the surface of the particles seems act as a lubricant against mechanical friction.

In addition, according to this work, the HME process was able to transform the starting IND crystalline phase in a mixture of the amorphous with metastable crystalline phases (alpha and others). Despite a change in the solid state, the EG samples were more soluble and showed an improvement on IND dissolution kinetics compared to commercial γ-IND. Apparent solubility with values 1.5 times greater than the equilibrium concentration with γ-IND can be partly attributed to the surfactant effect, but it is mainly related to amorphous phase and to different polymorphic forms present in different samples. The other performance of interest is the dissolution kinetic profile. According to results, the solid dispersions freshly produced showed a dissolution profile similar to the immediate release solid dosage forms for different drug loads and for both Sepitrap™ grades. Direct exposure of the samples with a high drug load (40% wt) to a stressful environment of temperature and humidity (40 °C, 75%RH) in open vials showed a slightly decrease of solubility from 12 weeks. However, no sample evolved to the γ form during extreme accelerated storage conditions. Solid dispersion formulations with both grades of Sepitrap™ avoided the transformation from amorphous metastable crystalline forms to the stable crystalline form.

To summarize, this study shows that Sepitrap™ can open new opportunities for the formulation and improvement of bioavailability of poorly soluble active ingredients in the form of solid dispersions with a high drug load generated by hot melt extrusion, in granule form, without shaping post-processing (grinding or otherwise), which represents an advantage in terms of the process of producing solid dispersions and formulation stability. This study will be extended to other BCS class II molecules.

Acknowledgements

The authors are grateful to P. Accart, L. Devrient, V. Nallet and C. Rolland from Rapsodee Center for respectively particle size, dissolution tests, XRPD analyses and SEM images and to Gala Platform Team for extrusion tests.

Disclosure statement

No potential conflict of interest was reported by the author(s). The authors report no conflicts of interest. The authors alone are responsible for the content and writing of the paper.

Funding

Research reported in this publication was supported by SEPPIC S.A.

References

Ambrus R, Alshweiat A, Szabó-Révész P, Bartos C, Csóka I. 2022. Smartcrystals for efficient dissolution of poorly water-soluble meloxicam. Pharmaceutics. 14(2):245. doi: 10.3390/pharmaceutics 14020245.

Davis MT, Potter CB, Walker GM. 2018. Downstream processing of a ternary amorphous solid dispersion: the impacts of spray drying and hot melt extrusion on powder flow, compression and dissolution. Int J Pharm. 544(1):242–253. doi: 10.1016/j.ijpharm.2018.04.038.

El-Setouhy DA, Basalious EB, Abdelmalak NS. 2015. Bioenhanced sublingual tablet of drug with limited permeability using novel surfactant binder and microencapsulated polysorbate: in vitro/in vivo evaluation. Eur J Pharm Biopharm. 94:386–392. doi: 10.1016/j.ejpb.2015.06.006.

FDA. 2018. *Dissolution Testing and Acceptance Criteria for Immediate-Release Solid Oral Dosage Form Drug Products Containing High Solubility Drug Substances. Guidance for Industry*. https://www.fda.gov/regulatory-information/search-fda-guidance-documents/dissolution-testing-and-acceptance-criteria-immediate-release-solid-oral-dosage-form-drug-products

Jagtap S, Magdum C, Jagtap R. 2021. Ameliorated Solubility and Dissolution of Flurbiprofen using Solubilizer Sepitrap 80 and Sepitrap 4000. Res J Pharm Technol. 14(1):21–27. doi: 10.5958/0974-360X.2021.00005.6.

Luebbert C, Sadowski G. 2017. Moisture-induced phase separation and recrystallization in amorphous solid dispersions. Int J Pharm. 532(1):635–646. doi: 10.1016/j.ijpharm.2017.08.121.

Morsi RE, Mohamed RS. 2018. Nanostructured mesoporous silica: influence of the preparation conditions on the physical-surface properties for efficient organic dye uptake. R Soc Open Sci. 5(3):172021. doi: 10.1098/rsos.172021.

Német Z, Sztatisz J, Demeter Á. 2008. Polymorph transitions of bicalutamide: a remarkable example of mechanical activation. J Pharm Sci. 97(8):3222–3232. doi: 10.1002/jps.21256.

Okumura T, Ishida M, Takayama K, Otsuka M. 2006. Polymorphic transformation of indomethacin under high pressures**The previous affiliation when this study was done, organic synthesis research laboratory, Sumitomo Chemical Co., Ltd. 3-1-98, Kasugade-naka, Konohana-ku, Osaka 554-8558, Japan. J Pharm Sci. 95(3):689–700. doi: 10.1002/jps.20557.

Pandi P, Bulusu R, Kommineni N, Khan W, Singh M. 2020. Amorphous solid dispersions: an update for preparation, characterization, mechanism on bioavailability, stability, regulatory considerations and marketed products. Int J Pharm. 586: 119560. doi: 10.1016/j.ijpharm.2020.119560.

Prasetyo AB, Handayani M, Sulistiyono E, Syahid AN, Febriana E, Mayangsari W, Muslih EY, Nugroho F, Firdiyono F. 2022. Development of high purity amorphous silica from emulsifier silicon by pyrolysis process at temperature of 700° C. J Phys: conf Ser. 2190(1):012013. doi: 10.1088/1742-6596/2190/1/012013.

Rumondor ACF, Stanford LA, Taylor LS. 2009. Effects of polymer type and storage relative humidity on the kinetics of felodipine crystallization from amorphous solid dispersions. Pharm Res. 26(12):2599–2606. doi: 10.1007/s11095-009-9974-3.

Surwase SA, Boetker JP, Saville D, Boyd BJ, Gordon KC, Peltonen L, Strachan CJ. 2013. Indomethacin: new polymorphs of an old drug. Mol Pharm. 10(12):4472–4480. doi: 10.1021/mp400299a.

Van Duong T, Lüdeker D, Van Bockstal P-J, De Beer T, Van Humbeeck J, Van den Mooter G. 2018. Polymorphism of indomethacin in semicrystalline dispersions: formation, transformation, and segregation. Mol Pharm. 15(3):1037–1051. doi: 10.1021/acs.molpharmaceut.7b00930.

Vo CL-N, Park C, Lee B-J. 2013. Current trends and future perspectives of solid dispersions containing poorly water-soluble drugs. Eur J Pharm Biopharm. 85(3 Pt B):799–813. doi: 10.1016/j.ejpb.2013.09.007.

Xu T, Nahar K, Dave R, Bates S, Morris K. 2018. Polymorphic transformation of indomethacin during hot melt extrusion granulation: process and dissolution control. Pharm Res. 35(7):140. doi: 10.1007/s11095-017-2325-x.

Yang Z, Nollenberger K, Albers J, Qi S. 2014. Molecular implications of drug–polymer solubility in understanding the destabilization of solid dispersions by milling. Mol Pharm. 11(7):2453–2465. doi: 10.1021/mp500205c.

Zhang X, Xing H, Zhao Y, Ma Z. 2018. pharmaceutical dispersion techniques for dissolution and bioavailability enhancement of poorly water-soluble drugs. Pharmaceutics. 10(3):74. doi: 10.3390/pharmaceutics10030074.